Title
Raising the Speed Limit for β-Hairpin Formation

Journal
Journal of the American Chemical Society, 134(35)

ISSN
0002-7863

Authors
Davis, Caitlin M
Xiao, Shifeng
Raleigh, Daniel P
et al.

Publication Date
2012-09-05

DOI
10.1021/ja3046734

Peer reviewed

Published in final edited form as:
J Am Chem Soc. 2012 September 5; 134(35): 14476–14482. doi:10.1021/ja3046734.

Raising the Speed Limit for β-Hairpin Formation

Caitlin M. Davis[†], **Shifeng Xiao**[‡], **Daniel P. Raleigh**[‡,*], and **R. Brian Dyer**[†,*]

[†]Department of Chemistry, Emory University, Atlanta, Georgia 30322, United States

[‡]Department of Chemistry, State University of New York, Stony Brook, New York 11794, United States

Abstract

Understanding the folding of the β-hairpin is a crucial step in studying how β-rich proteins fold. We have studied CLN025, an optimized ten residue synthetic peptide, which adopts a compact, well-structured β-hairpin conformation. Formation of the component β-sheet and β-turn structures of CLN025 was probed independently using a combination of equilibrium Fourier transform infrared spectroscopy and laser-induced temperature jump coupled with time-resolved infrared and fluorescence spectroscopies. We find that CLN025 is an ultrafast folder due to its small free energy barrier to folding and that it exceeds the predicted speed limit for β-hairpin formation by an order of magnitude. We also find that the folding mechanism cannot be described by a simple two-state model, but rather is a heterogeneous process involving two independent parallel processes. Formation of stabilizing cross-strand hydrophobic interactions and turn alignment occur competitively, with relaxation lifetimes of 82 ± 10 and 124 ± 10 ns, respectively, at the highest probed temperature. The ultrafast and heterogeneous folding kinetics observed for CLN025 provide evidence for folding on a nearly barrierless free energy landscape, and recalibrate the speed limit for the formation of a β-hairpin.

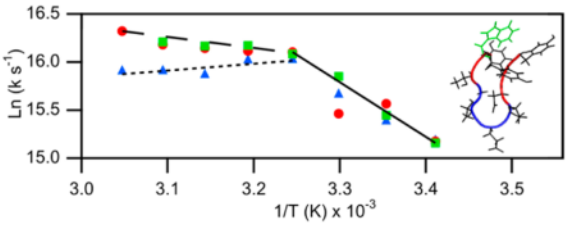

INTRODUCTION

Small single-domain peptides that fold quickly provide experimental models that are useful for studying the fundamental principles of protein folding.[1,2] Peptide models of both α-helix and β-sheet have provided important insight about the stability and dynamics of these secondary structures. Extensive studies of model α-helical peptides show that the rate of formation of the α-helix is fast, with a characteristic lifetime on the sub-microsecond time scale.[3–5] Similar studies on model β-hairpin peptides reveal slower folding rates that span a wide range.[6–8] These differences can be understood in terms of the speed limit for the

Corresponding Author: briandyer@emory.edu; draleigh@notes.cc.sunysb.edu.

Supporting Information
CD spectra and CD melt curves fit to a two-state model. This material is available free of charge via the Internet at http://pubs.acs.org.

Notes
The authors declare no competing financial interest.

formation of each secondary structural element, a concept that emerges from the free energy landscape theory of protein folding. The speed limit for folding is a consequence of folding on a smooth, funneled free energy landscape with a minimal free energy barrier to folding.[9] Eaton introduced the important concept of a speed limit for β-hairpin formation based on the minimum chain collapse time to form stabilizing cross-strand interactions (between residues that are far apart in sequence), whereas the rate of helix formation is limited by the helix nucleation time, determined by local interactions. Therefore, the speed limit for β-hairpin formation is estimated to be ~10^6 s^{-1}, approximately 10-fold slower than the speed limit of α-helix formation.[10] These ideas have been difficult to test experimentally. Proteins often exhibit two-state folding behavior, meaning they fold on an energy landscape with a single dominant energy barrier. Two-state folders exhibit simple single-exponential kinetics, representing population flow over the barrier, without providing any microscopic insight into the reaction progress. The same rate is observed regardless of the structural probe employed. But folding in the absence of a barrier should occur at the speed limit, and in this case it should be possible to observe the progressive development of the folded structure directly, revealing the complexity and heterogeneity of the process. Thus, a defining characteristic of folding at or near the speed limit should be non-two-state folding behavior.

The β-hairpin is the simplest β-sheet structural motif, and it is often found in larger β-sheets in globular proteins. It is possible to form soluble and stable β-hairpins from isolated short peptides,[11] supporting the idea that they may act as nucleation sites for folding more complex β-sheet structures. Small fast-folding model β-hairpins are ideal candidates for protein folding studies of β-proteins, because the folding dynamics of these systems occur on a time scale where experiment and all-atom molecular dynamic simulations overlap with each other. Previously, we have measured relaxation kinetics of model β-hairpins using laser-induced temperature jump (T-jump) and time-resolved infrared (IR) and fluorescence spectroscopy.[12,13] Similar methods have been used by a number of groups to study the folding of β-hairpins. Using fluorescence T-jump, Yang et al. reported wavelength-dependent relaxation lifetimes of trpzip2 on the microsecond time scale.[14] Xu et al. studied folding kinetics of a 15-residue β-hairpin that folds within 800 ns at 300 K.[15] Our results for a series of cyclic β-hairpin analogues of Gramidicin S exhibited relaxation lifetimes ($\tau \approx$ 100 ns) independent of chain length, much faster than those reported for linear β-hairpins.[12] These results suggest that the folding rates of β-hairpins are not uniform, but rather are dependent on many factors, particularly the specific type of turn structure and the rate of chain collapse.

The CLN025 β-hairpin (YYDPETGTWY, Figure 1) is a good model system for further investigation of β-hairpin folding dynamics, because its stability and small size are ideal for ultrafast folding experiments. CLN025 is a member of the designed Chignolin family of peptides. The parent Chignolin is a 10-residue β-hairpin derived from the 16-residue β-hairpin G-peptide. [17] The internal eight residues of Chignolin were statistically optimized to form a stable β-hairpin using a databank of over 10 000 peptide sequences.[18] The terminal residues of Chignolin were further optimized to design CLN025.[16] Computational studies on Chignolin and CLN025 have predicted folding lifetimes of hundreds of nanoseconds,[19,20] the same time scale as the fastest previously reported β-hairpins. Computational studies have not agreed on the folding mechanism of Chignolin with one study reporting the turn forming first[21] and another reporting hydrophobic collapse as the first step.[22] MD simulations of CLN025 folding by Lindorff-Larsen et al. predict hairpin formation along multiple folding pathways.[20] These predictions for Chignolin and CLN025 mirror the general state of understanding of β-hairpin formation. Two different models have been proposed, one initiated by hydrophobic and the other by hydrogen bonding interactions.[23] In the first model, the turn zipper mechanism postulated by Muñoz et al., folding is initiated in the turn region and zipped from the turn to the end.[3,24,25] Dinner et al. proposed an alternative

model, the hydrophobic collapse mechanism, which predicts hydrophobic collapse prior to formation of hydrogen bonds and the hairpin.[6–8]

We have studied the dynamics of β-turn formation and hydrogen bond propagation in CLN025 using T-jump, time-resolved IR spectroscopy. Pulsed laser excitation was used to rapidly initiate a shift in the folding equilibrium. The relaxation dynamics of CLN025 were measured by independently probing the amide I components assigned to turn formation and β-sheet formation. The IR studies were complemented by fluorescence T-jump experiments that probe tryptophan (Trp) side-chain dynamics.[26] We find that CLN025 folds much faster than any previously studied linear β-hairpin, consistent with the time scale predicted by computations.[19,20] We find that CLN025 has a small free energy barrier to folding and the observed folding rate exceeds the predicted speed limit, likely because chain collapse is not rate limiting in this case. Instead of a dominant pathway involving either turn formation or hydrophobic collapse as a rate limiting step, we observe heterogeneous folding rates that depend on the specific structural probe. Using multiple spectroscopic probes we observe formation of stabilizing cross-strand hydrophobic interactions and turn formation occurring in parallel but on slightly different time scales. The ultrafast and heterogeneous folding kinetics provide evidence for folding at the speed limit on a nearly barrierless free energy landscape.

EXPERIMENTAL SECTION

Protein Synthesis and Purification

The CLN025 peptide, YYDPETGTWY,[16] was synthesized via standard 9-fluornylmethoxycarbonyl (Fmoc)-based solid-phase chemistry. Fmoc-Tyr(tBu)-PEGPS resin was used to form a free C-terminus. The peptide was purified by reverse-phase high-pressure chromatography. HCl was used as the counterion to reduce the residual TFA concentration since TFA can interfere with Amide-I IR measurements at 1672 cm^{-1}. The identity of the peptide was confirmed by matrix-assisted laser desorption ionization time-of-flight mass spectrometry. The peptide was lyophilized and dissolved in D_2O to allow deuterium–hydrogen exchange of the amide protons. The peptide was lyophilized a second time and resuspended in a filtered D_2O buffer with 20 mM potassium phosphate and 150 mM sodium chloride at pH 7.0. Sample concentrations of 0.5–6 mM were prepared for both IR and fluorescence experiments.

Fourier Transform Infrared (FTIR) Spectroscopy

The equilibrium melting behavior was monitored on a Varian Excalibur 3100 FTIR spectrometer (Varian Inc., Palo Alto, CA) using a temperature-controlled IR cell. The IR cell consists of two CaF_2 windows stacked and separated by a 100 μm Teflon spacer split into two compartments, a sample and a reference. The same cells are used for equilibrium FTIR and T-jump experiments. No aggregation was observed (characteristic amide I′ bands indicative of aggregation were not observed) at reported concentrations. All spectra shown at a specific temperature are constructed by subtracting the spectrum of reference buffer solution without protein from sample solution with protein. The temperature-dependent difference spectra were then generated by subtracting the spectrum at 5 °C from the spectra at higher temperatures. The temperature-dependent difference spectra were baseline corrected in the amide I′ region from 1500 to 1750 cm^{-1} using a linear baseline to account for the baseline differences caused by slight differences in H_2O concentration. The second derivative spectra were computed in IGOR PRO (WaveMetrics, Lake Oswego, OR). The reported spectra are not smoothed and have a signal-to-noise level greater than 10:1. Comparison to the second derivative spectrum of water vapor indicates the protein spectra are free from water vapor artifacts (Figure S3).

Time-Resolved Temperature Jump Relaxation Measurements

The T-jump apparatus has been described previously.[25] Pulsed laser excitation is used to rapidly perturb the folding equilibrium on a time scale faster than the molecular dynamics of interest. Time resolved IR or fluorescence is then used to probe the reaction. A Q-switched DCR-4 Nd:YAG laser (Spectra Physics, Mountainview, CA) fundamental at 1064 nm is Raman shifted (one stokes shift in 200 psi H_2 gas) to produce a 10 ns pulse at 2 μm. The magnitude of the T-jump is calculated using the change in reference absorbance with temperature. The T-jump reference is taken from the 6 mM sample at a frequency, 1680 cm^{-1}, that is temperature independent for the peptide based on the equilibrium FTIR studies. Absorbance changes at the reference wavelength are only due to changes in D_2O absorbance, which is used as an internal thermometer.[25]

The change in signal induced by the T-jump is probed in real time by a continuous laser with a wavelength either in the amide I′ band of the IR or at 285 nm to excite Trp fluorescence. The mid-IR probe beam is generated by a continuous wave quantum cascade laser (Daylight Solutions Inc., San Diego, CA) with a tunable output range of 1535–1695 cm^{-1}. The transient transmission of the probe beam through the sample is measured using a fast, 100 MHz, photovoltaic MCT IR detector/preamplifier (Kolmar Technologies, Newburyport, MA). Transient signals are digitized and signal averaged (5000 shots) using a Tektronics digitizer (7612D, Beaverton, OR).

The fluorescence excited at 285 nm and collected from 320 to 370 nm is sensitive to changes in the tryptophan residue near the C-terminus of the peptide. A Verdi V12 DPSS high-power continuous-wave laser (Coherent, Santa Clara, CA) is used to pump a Mira 900 Ti:sapphire laser (Coherent) which produces a quasi-continuous beam at 855 nm. The beam is then passed through a second and third harmonic generator (Coherent) to produce the fluorescence probe beam at 285 nm. The back-emitted fluorescence light induced by the 285 nm pump laser is measured through a 355 ± 15 nm band-pass filter using a Hamamatsu R7518 photomultiplier tube (Hamamatsu Photonics K.K., Hamamatsu City, Japan), digitized, and signal averaged (10 000 shots) using a Tektronics digitizer (7612D, Beaverton, OR). A 400 μM tryptophan (Trp) solution in D_2O is used as a reference to measure the magnitude of the T-jump and determine the temperature dependence of the tryptophan signal. Instrument control and data collection are controlled using a LabVIEW computer program.

Analysis of Kinetics Data

A D_2O reference is collected for each sample measurement at each temperature. The relaxation lifetime of the reference signal is the instrument response of the sample. In order to minimize detector artifacts, the reference is scaled prior to subtraction from the sample. This process leaves a small residual signal from the instrument response. Due to the fast time scale, accurate determination of the peptide relaxation kinetics requires a deconvolution of the instrument response function from the observed kinetics. Standard deconvolution methods were unable to accurately deconvolve the instrument response from the relaxation kinetics because of fast time scale artifacts in the data. Instead the instrument response and peptide relaxation kinetics were fit to a biexponential function given as

$$y=A_0+A_1\left(\frac{-(x-x_0)}{\tau_1}\right)+A_2\exp\left(\frac{-(x-x_0)}{\tau_2}\right) \quad (1)$$

where A_0 is an offset, A_1 and A_2 are preexponential factors, τ_1 is the instrument response, τ_2 is the relaxation lifetime of the sample, and x is the time. The data was fit to a

biexponential function and the first relaxation lifetime, corresponding to the instrument response, was averaged over all temperatures to get a global instrument response value. In a second set of fits to the biexponential function the first relaxation lifetime was fixed to the global instrument response value, 20 ns for IR T-jumps and 50 ns for fluorescence T-jumps, both in good agreement to the previously reported instrument response time of ~20 ns.[27] The reported kinetics are from the second relaxation lifetime in the biexponential function. All data was fit from 10^{-8} to 2×10^{-6} s. The data analysis was performed in IGOR PRO (WaveMetrics, Lake Oswego, OR).

RESULTS

Equilibrium FTIR Studies

The temperature-induced unfolding of CLN025 was studied over the range from 5 to 85 °C in 5 °C intervals using FTIR spectroscopy to monitor the amide I′ region. The amide I′ spectral region (amide I region of peptides in D_2O), composed of mostly C=O stretching vibrations of the polypeptide backbone carbonyls, is an established indicator of secondary structure.[28–30] The absorption spectra of the amide I′ region as a function of temperature are shown in Figure 2A. This relatively broad band contains contributions from the entire polypeptide backbone, which in the case of the β-hairpin is made up of contributions from the β-sheet, the β-turn, or any random coil regions. The changes with temperature are highlighted in the difference spectra for each peptide, in Figure 2B. The difference spectra are generated by subtracting the lowest temperature spectrum from each absorbance spectrum at higher temperature. Negative peaks correspond to specific structures or interactions present in the folded state; the strongest of these are the peaks at 1614 and 1629 cm^{-1}. Positive peaks correspond to new interactions with solvent in the unfolded state; the characteristic feature due to the disordered polypeptide is a relatively broad peak, located at 1660 cm^{-1}.[3,25,31] The broad nature of these peaks may conceal some of the bands due to ordered structure. Spectral interpretation was aided by taking the second derivative of the FTIR spectra (Figure 2C) to uncover otherwise indistinguishable features.

The analysis revealed five components of the amide I′ band at 20 °C, centered near 1614, 1629, 1649, 1658, and 1678 cm^{-1} (Figure 2C). The intensity of these features decreases with increasing temperature, meaning these features are all associated with the folded state. The Keiderling group identified a characteristic peak at ~1611 cm^{-1} in β-hairpins with a proline in the turn, which they attributed to a tertiary amide linkage between the proline and the side chain of a neighboring amino acid.[32] Similarly, we assign the peak at 1614 cm^{-1} to a tertiary amide linkage between the backbone of glutamic acid and the side chain of aspartic acid in the turn (Figure 1).[18] Two peaks are observed for the β-sheet, corresponding to the inter- and intramolecular hydrogen-bonded carbonyl groups.[12] The peak at 1629 cm^{-1} is assigned to the inward directed carbonyl groups (Figure 1) and the peak at 1678 cm^{-1} is assigned to the solvent-exposed carbonyl groups. These assignments are supported by several pieces of evidence.

The FTIR spectral amide I′ absorbance maximum at 1629 cm^{-1} agrees with the well-documented indicator of cross-strand β-sheet interaction at 1634 cm^{-1}.[32] Most of the amide carbonyl groups are located in the sheet portion of the hairpin: there are six sheet carbonyls, four of which participate in intramolecular hydrogen bonds and two in intermolecular hydrogen bonds to water, as opposed to three carbonyls in the turn, involved in one tertiary amide, one intramolecular and one intermolecular hydrogen bond to water, respectively. The relative intensities of the sheet and turn bands support these assignments if the individual C=O groups are assumed to act as local oscillators and have similar oscillator strengths. The high frequency bands at 1649, 1658, and 1678 cm^{-1} overlap with the broad positive absorbance centered at 1660 cm^{-1} that grows in with increasing temperature in the

difference spectra. This broad random coil peak is composed of carbonyl groups hydrogen bonded to water, so solvent exposed carbonyls in the folded structure are also expected to have similar frequency. The additional two peaks at 1649 and 1658 cm^{-1} cannot be positively identified, however, they most likely correspond to β-turn carbonyls with different degrees of solvent exposure or interaction.[32]

The melting curve derived from the temperature dependent IR absorbance at 1629 cm^{-1} is shown in Figure 3. To test whether the peptide exhibits a simple two-state behavior, the data are fit to an apparent two-state equilibrium model:

$$A=\frac{A_i+A_f\times 10^{2(T-T_m)/\Delta T}}{1+10^{2(T-T_m)/\Delta T}} \quad (2)$$

where A_i and A_f are the extrapolated absorbance values at the two end points of the transition, T_m is the transition midpoint, and ΔT represents the overall temperature range of the transition. The T_m and ΔT values from the two-state model fit are listed in Table 1. The melting temperature of the β-sheet, 70.9 ± 1.8 °C, agrees well with the previously reported melting temperature obtained by circular dichroism, 69.9 °C.[16] The melt curve derived from other wavelengths agreed with the melting temperature within error of the fit. The relatively sharp transition (small ΔT) reveals that the melt is cooperative.[12] Apparent thermodynamic parameters (assuming a two-state model) derived from a van't Hoff analysis (inset of Figure 3) are also summarized in Table 1. A van't Hoff plot of the log of the observed equilibrium constant versus $1/T$ should be linear. The van't Hoff analysis reveals a pre-transition below 35 °C, showing that hairpin folding is not a simple two-state process. The nonlinear behavior cannot be explained by a heat capacity change upon unfolding. It is unlikely that such a small structure would have a large difference in heat capacity between the folded and unfolded states, however, if it did it would have a parabolic dependence on temperature, which does not agree with the observed line shape. Previous studies on Chignolin, which is the parent of CLN025, reported a $\Delta C_p \approx 0$.[18] Thermodynamic parameters were obtained by treating the pretransition, below 35 °C, and transition, above 35 °C, as two independent two-state processes. The enthalpy gain and entropic cost for the higher temperature transition are nearly double those of the lower temperature one. Both theoretical and experimental studies have shown that vibrational spectroscopy can be sensitive to solvent interaction with the peptide backbone.[33] Therefore we assign the low temperature transition, with its relatively small enthalpic difference to a subtle global change in solvent interaction. In contrast, the higher temperature transition with a larger enthalpic change is clearly due to the hairpin folding.

Temperature-Jump Relaxation Kinetics

The probedependent relaxation kinetics of the folding/unfolding transition following a laser-induced T-jump were probed using time-resolved IR spectroscopy of the amide I′ frequency for the tertiary amide of the turn (1619 cm^{-1}) and the β-sheet (1629 cm^{-1}). Jumps in the turn region were performed slightly off the peak center (1614 cm^{-1}) to maximize the signal. Kinetic experiments examined the dependence of the relaxation rates on the final temperature following a T-jump. The magnitude of the T-jump was kept constant while varying the final temperature with all final temperatures below the melting transition. Figure 4 shows the results for a T-jump from 40 to 55 °C probed by IR absorbance. The transients were fit to a double exponential. The first relaxation lifetime for all jumps corresponds to the solvent response, which occurs within the instrument response time, and the second lifetime, which decreases with increasing temperature, corresponds to the relaxation lifetime of the specific peptide structure being probed. The relaxation kinetics observed for the peptides are reported in Table 2. At low final jump temperatures there is little difference between the turn

and β-sheet kinetics. As the final jump temperatures increase, the turn relaxation lifetimes, probed at 1619 cm^{-1}, stabilize at 124 ± 10 ns. The β-sheet lifetimes, probed at 1629 cm^{-1}, continue to decrease throughout the entire series of jumps with a relaxation lifetime at the final jump temperature of 82 ± 10 ns significantly faster than the relaxation lifetimes observed in the turn. The difference in the relaxation lifetimes observed in the turn and the sheet is well outside the error in the measurements. Because the final temperature of all jumps is at least 15 °C below the melting temperature, the folding rate will dominate the observed relaxation kinetics.

A second set of kinetics experiments with a series of similar magnitude jumps were performed using time-resolved fluorescence. There is a tryptophan located near the terminus of the hairpin, so the tryptophan fluorescence intensity is sensitive to changes in the β-sheet structure and hydrophobic packing of the core of the hairpin (Figure 1). Figure 5 shows the results for a T-jump from 15 to 25 °C probed by fluorescence emission. Similar to the IR T-jumps, we observe an instrument limited response component (due to the intrinsic temperature dependence of the Trp fluorescence quantum efficiency) in addition to the fluorescence relaxation kinetics (Table 2). As expected, the fluorescence probed relaxation lifetimes are similar to the IR probed relaxation lifetimes of the β-sheet.

Both fluorescence and IR probed jumps had a final jump temperature below the melting transition, so the observed kinetic rates are dominated by the folding rate. If the β-hairpin followed two-state folding kinetics, an Arrhenius plot (Figure 6) of the natural log of the measured rate constants versus $1/T$ should be linear for the case where there is no heat capacity change upon folding. The Arrhenius plot shows three distinct regions separated by temperature and probed region of the peptide. The kinetics observed for the fluorescence or the IR probed at 1629 cm^{-1} is sensitive to changes in the sheet, whereas the kinetics probed by IR at 1619 cm^{-1} is sensitive to changes in the turn. The break in temperature occurs at 35 °C, the same break that was observed in the equilibrium van't Hoff analysis. The observed activation energy in this region is the same for all fluorescence and IR probed kinetics. This supports the conclusion from the van't Hoff analysis that there is a global change that affects both the turn and β-sheet at lower temperatures, since both the turn and β-sheet experience the same activation energy. Above 35 °C the Arrhenius plot shows different behavior depending on the region of the peptide that is probed. The β-sheet region exhibits faster kinetic rates and a small apparent activation energy. The turn region shows a slower kinetic rate and an apparent activation energy near zero. This analysis does not account for the temperature dependence of the viscosity of the solution.

DISCUSSION

Simple peptide models are valuable as a basis for understanding the fundamental processes of protein folding that lead to the complex architecture of globular proteins. β-hairpins are the simplest structural motif of a β-protein, and yet their folding mechanism is not fully understood. Previous protein folding studies predict β-hairpin formation to follow a turn zipper mechanism or a hydrophobic collapse mechanism and to fold with a speed limit that is significantly slower than that of α- helix.[3,23–25] We have studied these issues for the CLN025 peptide, an optimized β-hairpin structure with a unique hydrophobic cluster at its terminus.

A van't Hoff analysis is used to gain insight into the nature of the thermally induced transition. Over the temperature range from 5 to 85 °C we observe a global pre-transition at low temperature. The enthalpy gain and entropic cost at higher temperature are nearly double those at lower temperature. The apparent thermodynamic parameters are similar to those found previously for a 10-residue cyclic hairpin (ΔH° = −48.3 kJ mol^{-1}, ΔS° =

−140.4 J mol^{-1} K^{-1}).[12] Making the assumption that the thermodynamic parameters at higher temperature (but still well below T_m) are the thermodynamic parameters of folding, the entropy loss of folding of CLN025 is 30% greater than that of a cyclic peptide. The cyclization study showed that side chain motions dominate the entropy change in the constrained peptide. CLN025 likely has a similar contribution to ΔS from side-chain motions; however, we expect that there is an additional small entropic contribution from the peptide backbone motion since it is not fully constrained.

We used IR probes to study the relaxation kinetics of the turn (1619 cm^{-1}) and the sheet (1629 cm^{-1}), and a fluorescence probe to study relaxation kinetics of the tryptophan side chain. Previously, this multiple-probe approach was successfully used to probe the inter- and intramolecular hydrogen bonds in the villin headpiece subdomain.[34] We see a break between low- and high-temperature regions, at the same temperature as that observed in the van't Hoff analysis. At low temperatures we observe the same relaxation kinetics regardless of time-resolved probe, supporting the conclusion that this process is a global solvent rearrangement. At temperatures above the discontinuity we observe two sets of relaxation kinetics, depending on the region of the peptide that is probed. The folding kinetics cannot be fit with a simple two-state model. The relaxation lifetimes suggest that the β-sheet and turn form in parallel with slightly different rates, the β-sheet having a faster relaxation lifetime. Studies on type II′ β-turns have shown that the rate is dominated by the folding of the turn structure.[12] Our results support this analysis, and extend the observation to non-type II′ turns. The turn is found to have a near zero apparent activation energy, consistent with the ultrafast folding rate. Any remaining barrier to turn formation must be small and mostly entropic, a consequence of the search to find stabilizing contacts and the correct alignment of the turn.

The T-jump relaxation kinetics observed for CLN025 are three times faster than the fastest relaxation kinetics observed for other linear β-hairpins.[13,35] The observed relaxation rates are 2 orders of magnitude faster than those observed for the β- hairpin of protein G.[36] The β-hairpin of protein G provided a model for the derivation of CLN025.[16–18] The statistical optimization of the β-hairpin sequence appears to have greatly accelerated the folding of the peptide. The relaxation kinetics of CLN025 are on the same order as the relaxation kinetics of cyclic peptides.[12] In a cyclic β-hairpin the ends of the structure are "pinned" together (covalently bonded), restricting the accessible conformations in the unfolded state. This conformational restriction eliminates chain collapse as the rate-limiting step. The interactions between aromatic and hydrophobic groups at the termini of CLN025 may play a similar role and serve to severely restrict conformation space and help to drive folding by rapidly forming a collapsed structure. We postulate that there are residual interactions between these hydrophobic and π-stacking aromatics in the unfolded state that stabilize collapsed conformations in which the termini are pinned together, analogous to what is observed in cyclic hairpins, leading to similar folding dynamics. This model also explains why the folding rate exceeds the speed limit, because chain collapse is not the rate-limiting step.

The low activation barrier to β-hairpin formation allows us to observe subtle differences in the free energy landscape, depending upon how the reaction is probed. An Arrhenius plot of the different probe kinetics shows three distinct types of behavior. The Arrhenius plot shows that there is a small enthalpic barrier to β-sheet formation (9.6 ± 0.7 kJ/mol), whereas the barrier is near zero for turn formation. We emphasize that these are apparent barriers, because the Arrhenius analysis does not account for the temperature dependence of the viscosity of the solution. The apparent enthalpic barrier to β-sheet formation is likely due to the rearrangement of the hydrophobic interactions in the precollapsed state of the β-sheet of the hairpin. Although the activation energy is higher for the β-sheet than the turn, the

observed rates are still faster, which suggests that the entropic barrier for turn formation is higher than for β-sheet formation. Taken together, these results support a model in which residual hydrophobic interactions at the terminus create a compact structure that has the correct registry for sheet formation, but still requires a search to find the stabilizing contacts and the correct alignment of the turn.

MD simulations of CLN025 folding reported multiple folding pathways for β-hairpin formation.[20] In the majority of pathways reported the proline in the turn reached the native state first and the sheet formed later. An alternative pathway where the residues in the sheet reach the native state prior to the turn is also observed. There is little difference in average folding time predicted for the two observed pathways. IR T-jumps offer a way to validate theoretical models. Our experimental results on CLN025 support these computational studies by showing that there is no clear assignment of order of formation but rather that turn and β-sheet formation occur competitively. This suggests that β-hairpin formation cannot be described as a simple turn zipper or hydrophobic collapse mechanism, but rather is a complex combination of these models.

CONCLUSION

The study of CLN025 reveals that a simple two-state model cannot be used to describe the formation of this β-hairpin and that the speed limit for folding of β-hairpins is considerably faster than previously hypothesized. Linear β-hairpins have been reported to fold in a range from 800 ns to over 10 μs. Folding of CLN025 occurs as fast as ~100 ns, a similar time scale to cyclic β-hairpins and to α-helical peptides. The ultrafast folding rate is a consequence of a negligible global barrier to folding and requires a recalibration of the speed limit for β-hairpin formation. Previous estimates of the speed limit for the formation of a small 10-residue interchain loop were ~10^6 s^{-1}.[10,37] The relaxation lifetime observed for CLN025 breaks the speed limit by a factor of 10, and together with the heterogeneity in the kinetics indicates a smooth energy landscape with a minimal global barrier to folding. CLN025 folds as fast as α-helical peptides, demonstrating that β-hairpin formation may occur competitively with α-helical formation. Although a native-sequence β-hairpin that folds fast has not yet been discovered, this result at least provides proof of principle that β-hairpins can form quickly and therefore may act as nucleation sites for protein folding.

We propose a model to explain why CLN025 exceeds the previously proposed limit, based on residual interactions in the unfolded state between hydrophobic aromatic residues near the terminus. Such interactions lead to a pre-collapsed structure that only requires local rearrangements to reach the folded state. Furthermore, different relaxation lifetimes are observed based on the position probed in the β-hairpin. A fast rate and small apparent activation energy are observed when the hydrophobic cluster at the terminus is probed. Conversely, when the turn is probed a slightly slower rate and negligible activation energy are observed. The heterogeneous kinetics support a folding model in which the rate-limiting step of β-hairpin formation is stabilization of the collapsed system over a minimal barrier to achieve the native turn alignment. The observation of a small apparent enthalpic barrier further justifies this idea as it implies that the rate is limited by the registry search and stabilization of turn contacts. In summary, we have observed ultrafast folding and distinct structural dynamics in the turn and the sheet of CLN025 that show the folding of a simple ten residue β-hairpin is heterogeneous and not a simple two state process. The highly optimized CLN025 sequence establishes a new speed limit for β-hairpin formation on a nearly barrierless free energy landscape.

Supplementary Material

Refer to Web version on PubMed Central for supplementary material.

Acknowledgments

We thank Dr. Carlos Simmerling for helpful discussions. This work was supported by a grant from the National Institutes of Health (NIH R01 GM53640) to R.B.D. and a grant from the National Science Foundation (MCB-0919860) to D.P.R.

References

1. Eaton WA, Munoz V, Thompson PA, Henry ER, Hofrichter J. Acc Chem Res. 1998; 31:745–753.
2. Callender RH, Dyer RB, Gilmanshin R, Woodruff WH. Annu Rev Phys Chem. 1998; 49:173–202. [PubMed: 9933907]
3. Werner JH, Dyer RB, Fesinmeyer RM, Andersen NH. J Phys Chem B. 2002; 106:487–494.
4. Andersen NH, Fesinmeyer RM, Peterson ES, Dyer RB. Protein Sci. 2005; 14:2324–2332. [PubMed: 16131660]
5. Dyer RB, Causgrove TP. Chem Phys. 2006; 323:2–10.
6. Dinner AR, Lazaridis T, Karplus M. Proc Natl Acad Sci USA. 1999; 96:9068–9073. [PubMed: 10430896]
7. Klimov DK, Thirumalai D. Proc Natl Acad Sci USA. 2000; 97:2544–2549. [PubMed: 10716988]
8. Pande VS, Rokhsar DS. Proc Natl Acad Sci USA. 1999; 96:9062–9067. [PubMed: 10430895]
9. Bryngelson JD, Onuchic JN, Socci ND, Wolynes PG. Proteins: Struct, Funct Genet. 1995; 21:167–195. [PubMed: 7784423]
10. Kubelka J, Hofrichter J, Eaton WA. Curr Opin Struc Biol. 2004; 14:76–88.
11. Blanco FJ, Rivas G, Serrano L. Nat Struct Biol. 1994; 1:584–590. [PubMed: 7634098]
12. Maness SJ, Franzen S, Gibbs AC, Causgrove TP, Dyer RB. Biophys J. 2003; 84:3874–3882. [PubMed: 12770893]
13. Dyer RB, Maness SJ, Peterson ES, Franzen S, Fesinmeyer RM, Andersen NH. Biochemistry. 2004; 43:11560–11566. [PubMed: 15350142]
14. Yang WY, Gruebele M. J Am Chem Soc. 2004; 126:7758–7759. [PubMed: 15212506]
15. Xu Y, Oyola R, Gai F. J Am Chem Soc. 2003; 125:15388–15394. [PubMed: 14664583]
16. Honda S, Akiba T, Kato YS, Sawada Y, Sekijima M, Ishimura M, Ooishi A, Watanabe H, Odahara T, Harata K. J Am Chem Soc. 2008; 130:15327–15331. [PubMed: 18950166]
17. Honda S, Kobayashi N, Munekata E. J Mol Biol. 2000; 295:269–278. [PubMed: 10623525]
18. Honda S, Yamasaki K, Sawada Y, Morii H. Structure. 2004; 12:1507–1518. [PubMed: 15296744]
19. Kitao A. J Chem Phys. 2011:135.
20. Lindorff-Larsen K, Piana S, Dror RO, Shaw DE. Science. 2011; 334:517–520. [PubMed: 22034434]
21. Harada R, Kitao A. J Phys Chem B. 2011; 115:8806–8812. [PubMed: 21648487]
22. Suenaga A, Narumi T, Futatsugi N, Yanai R, Ohno Y, Okimoto N, Taiji M. Chem-Asian J. 2007; 2:591–598. [PubMed: 17465405]
23. Luo Z, Ding J, Zhou Y. J Chem Phys. 2008; 128:225103–255108. [PubMed: 18554060]
24. Munoz V, Henry ER, Hofrichter J, Eaton WA. Proc Natl Acad Sci USA. 1998; 95:5872–5879. [PubMed: 9600886]
25. Williams S, Causgrove TP, Gilmanshin R, Fang KS, Callender RH, Woodruff WH, Dyer RB. Biochemistry. 1996; 35:691–697. [PubMed: 8547249]
26. Dyer RB. Curr Opin Struct Biol. 2007; 17:38–47. [PubMed: 17223539]
27. Gulotta M, Rogatsky E, Callender RH, Dyer RB. Biophys J. 2003; 84:1909–1918. [PubMed: 12609893]
28. Yang WJ, Griffiths PR, Byler DM, Susi H. Appl Spectrosc. 1985; 39:282–287.

29. Arrondo JLR, Blanco FJ, Serrano L, Goni FM. FEBS Lett. 1996; 384:35–37. [PubMed: 8797798]
30. Susi H, Byler DM. Methods Enzymol. 1986; 130:290–311. [PubMed: 3773736]
31. Dyer RB, Gai F, Woodruff WH. Acc Chem Res. 1998; 31:709–716.
32. Hilario J, Kubelka J, Keiderling TA. J Am Chem Soc. 2003; 125:7562–7574. [PubMed: 12812496]
33. Wang L, Middleton CT, Zanni MT, Skinner JL. J Phys Chem B. 2011; 115:3713–3724. [PubMed: 21405034]
34. Brewer SH, Vu DM, Tang Y, Li Y, Franzen S, Raleigh DP, Dyer RB. Proc Natl Acad Sci USA. 2005; 102:16662–16667. [PubMed: 16269546]
35. Gai F, Xu Y, Oyola R. J Am Chem Soc. 2003; 125:15388–15394. [PubMed: 14664583]
36. Munoz V, Thompson PA, Hofrichter J, Eaton WA. Nature. 1997; 390:196–199. [PubMed: 9367160]
37. Hagen SJ, Hofrichter J, Eaton WA. J Phys Chem B. 1997; 101:2352–2365.

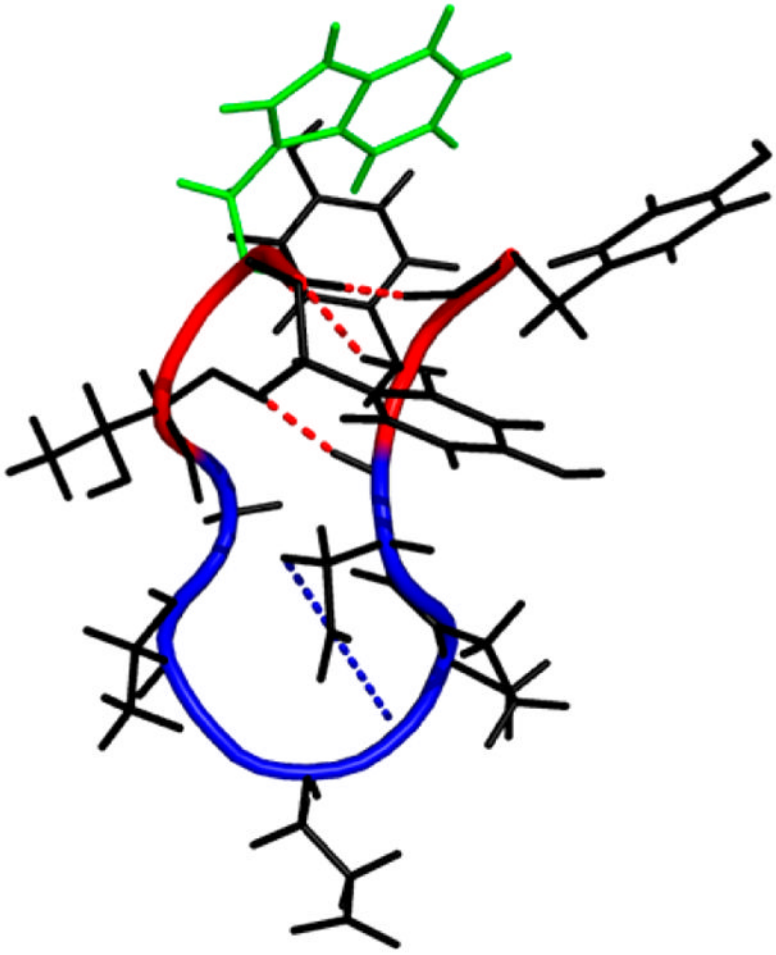

Figure 1.
Cartoon of the CLN025 crystal structure[16] with tertiary amide linkage in the turn (blue) highlighted with blue dashed line, intermolecular hydrogen bonded carbonyl groups in the β-sheet (red) highlighted by red dashed lines, and fluorescent tryptophan highlighted green.

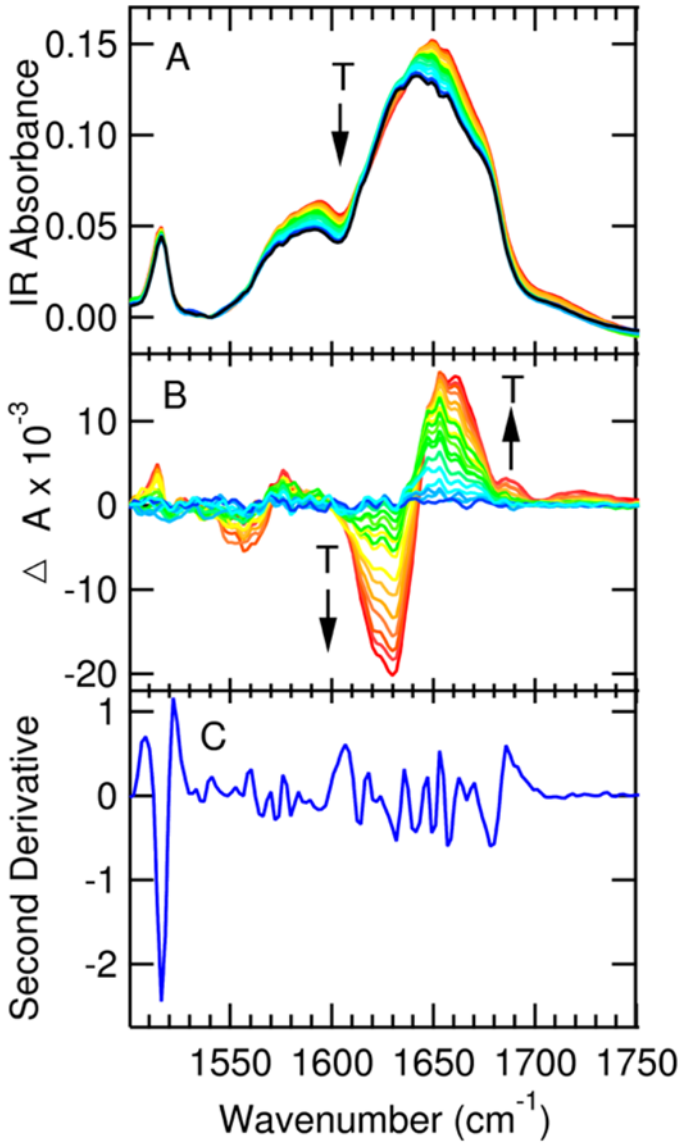

Figure 2.

Temperature-dependent FTIR spectra of 6 mM CLN025, in 20 mM potassium phosphate buffer (pH 7). (A) Absorbance spectra in the Amide I′ region; the temperatures of the individual traces varies from 5 to 85 °C from bottom to top in 5 °C intervals. (B) Baseline-corrected difference spectra obtained by subtracting the spectrum at 5 °C from the spectra at higher temperatures. (C) Second-derivative spectrum at 5 °C.

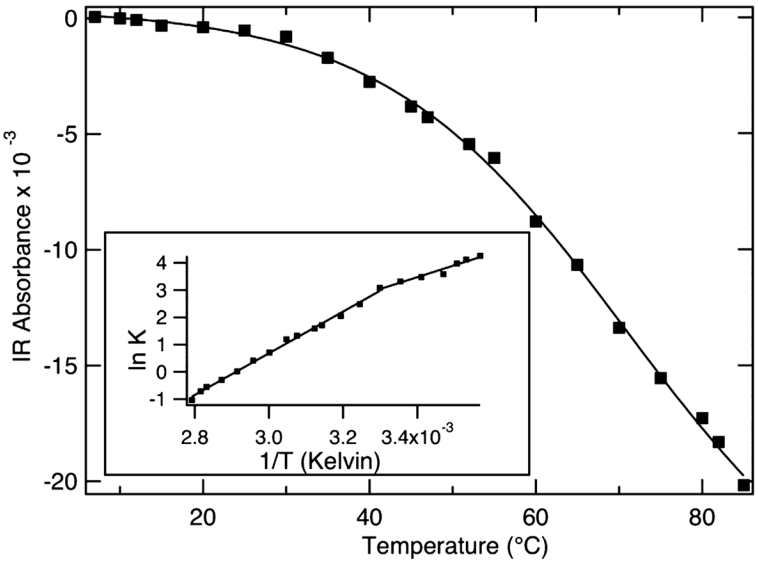

Figure 3.

FTIR melt curves for the CLN025 peptide obtained by plotting the change in the baseline corrected IR difference spectra intensity at the peak maximum of the β-sheet band at 1629 cm^{-1} versus temperature. The solid line is fit to a sigmoid (eq 1). Inset: Van't Hoff analysis using equilibrium constants generated from the melt curve.

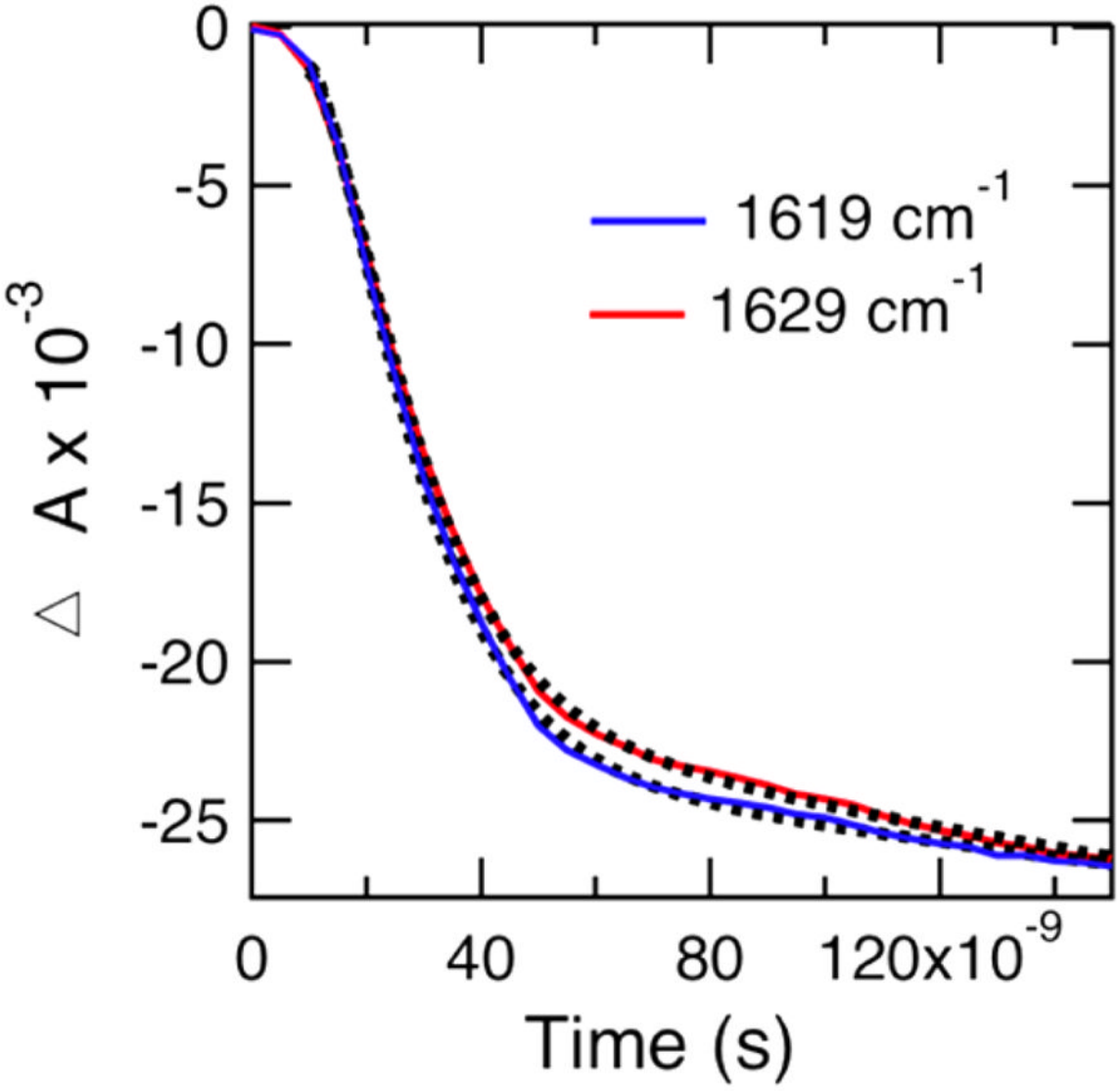

Figure 4.

Representative T-jump relaxation kinetics monitored in the amide I′ spectral region at 1619 (blue) and 1629 cm^{-1} (red) following a T-jump from 40 to 55 °C. A double exponential fit (dashed line) is overlaid on each kinetics trace. The amplitudes are normalized to the 1629 cm^{-1} amplitude at long time (4 μs) to aid comparison of the relaxation times.

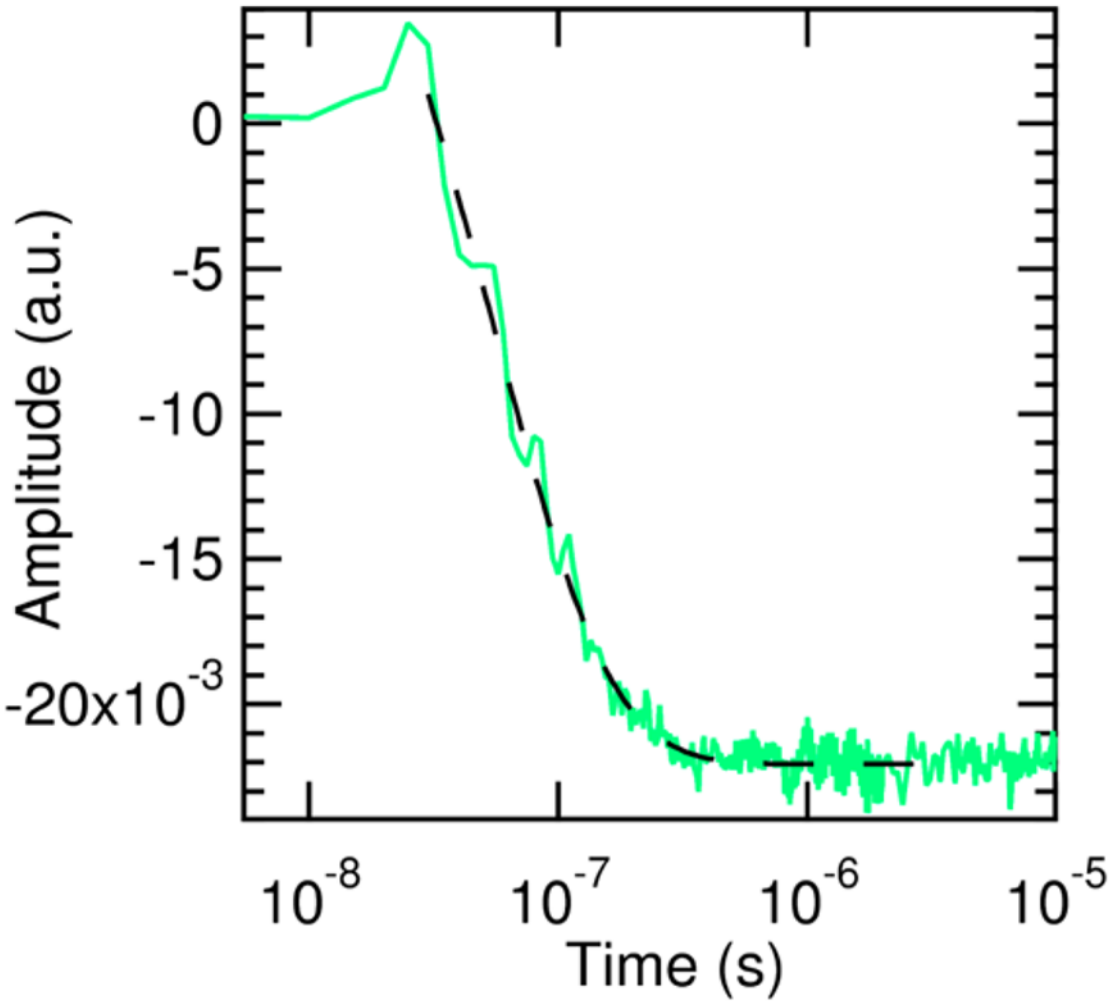

Figure 5.
Representative fluorescence T-jump relaxation kinetics excited at 285 nm and monitored at 350 nm following a jump from 15 to 25 °C. A double-exponential fit (dashed line) is overlaid on the kinetic trace.

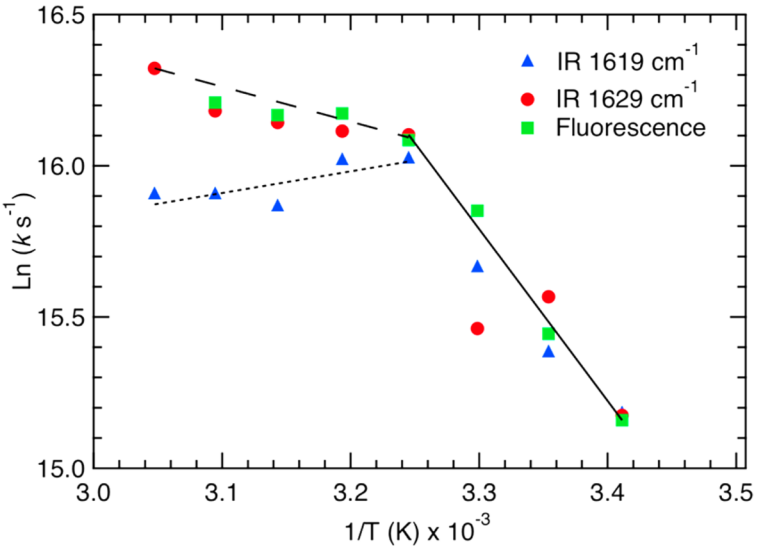

Figure 6.

Arrhenius plot of relaxation kinetics below T_m. The values of T used for the (1/T) axis are the final temperatures reached during the jump (all below T_m). k is the relaxation rate obtained from a fit (see text) of the T-jump transient fluorescenceor IR monitored at 1629 and 1619 cm^{-1}. Lines are the result of fitting all data (solid line), IR 1629 cm^{-1} and fluorescence (dashed line), and IR 1619 cm^{-1} (dotted line).

Table 1

CLN025 Thermodynamic Parameters of Folding

	T_m (°C)	ΔT (°C)	ΔH_f (kJ/mol)[a]	ΔS_f (J/mol·K)[a]
CLN025 <35 °C	70.9 ± 1.8	67.1 ± 4.1	−37.0 ± 1.5	−96.8 ± 5.1
CLN025 ≥35 °C	70.9 ± 1.8	67.1 ± 4.1	−62.8 ± 1.3	−182.8 ± 3.9

[a]Thermodynamic parameters are derived from a two-state model and a van't Hoff analysis.

Table 2

Relaxation Kinetics for CLN025

	τ_r (ns)			τ_r (ns)
IR T-jump, $\Delta T = T_i - T_f$ (°C)	**ν = 1619 cm^{-1}**	**ν = 1629 cm^{-1}**	**fluorescence T-jump, $\Delta T = T_i - T_f$ (°C)**	**λ_{em} = 350 nm**
5–20	256 ± 34	257 ± 30	10–20	261 ± 103
10–25	209 ± 23	173 ± 16	15–25	196 ± 44
15–30	158 ± 53	193 ± 44	20–30	131 ± 9
20–35	110 ± 8	107 ±7	25–35	103 ± 8
25–40	111 ± 8	100 ±8	30–40	95 ± 20
30–45	129 ± 14	98 ±8	35–45	95 ± 92
35–50	124 ± 10	94 ±8	40–50	91 ± 67
40–55	124 ± 10	82 ± 10		